



HAL
open science

Decrease of the spatial variability and local dimension of the Euro-Atlantic eddy-driven jet stream with global warming

Robin Noyelle, Vivien Guette, Akim Viennet, Bénédicte Colnet, Davide Faranda, Andreia Hisi, Pascal Yiou

► To cite this version:

Robin Noyelle, Vivien Guette, Akim Viennet, Bénédicte Colnet, Davide Faranda, et al.. Decrease of the spatial variability and local dimension of the Euro-Atlantic eddy-driven jet stream with global warming. *Climate Dynamics*, 2023, 10.1007/s00382-023-07022-z . hal-04337045

HAL Id: hal-04337045

<https://hal.science/hal-04337045v1>

Submitted on 11 Mar 2024

HAL is a multi-disciplinary open access archive for the deposit and dissemination of scientific research documents, whether they are published or not. The documents may come from teaching and research institutions in France or abroad, or from public or private research centers.

L'archive ouverte pluridisciplinaire **HAL**, est destinée au dépôt et à la diffusion de documents scientifiques de niveau recherche, publiés ou non, émanant des établissements d'enseignement et de recherche français ou étrangers, des laboratoires publics ou privés.

persistence and speed. We additionally observe a poleward shift of the jet. Our results suggest a zonalisation of the jet under global warming.

Keywords: jet stream, global warming, causal analysis, inter-decadal variability

1 Introduction

Jet streams are narrow, fast-flowing westerly air currents in the troposphere. They are a major feature of the large-scale atmospheric circulation and modulate the frequency, severity and persistence of weather events across the extratropics (Charney, 1947; Holton, 1973; Hurrell and Deser, 2010). Two types of atmospheric jets can be identified: thermally driven subtropical jets associated with the eastward deflection of the upper branch of the Hadley cell (Held and Hou, 1980), and eddy-driven jets caused by the transfer of energy from baroclinic eddies to the mean flow at the polar front (Held, 1975; Rhines, 1975). Real jets may arise from a combination of these mechanisms and thermally and eddy-driven jets are actually two limits in a continuous spectrum (Lee and Kim, 2003; Spensberger and Spengler, 2020; Messori et al, 2021).

Even though the climatological eddy-driven jet is mostly zonal flowing to the east, on a daily basis it can present large meanders. In these cases, the local flow becomes predominantly meridional or can even split or break. Those meanders have a typical spatial and temporal variability of a few thousand kilometers and of 10 days (Röthlisberger et al, 2016). The meanders allow air masses coming from the south or the north to persist around mid-latitude regions, potentially triggering temperature or precipitation extremes (Kautz et al, 2022). For its role in the triggering of extreme events in mid-latitude regions, the eddy-driven jet has been under great scrutiny in the past years.

The variability of the eddy-driven jet stream is an example of the large spontaneous variability of the climate system. The inter-decadal jet variability is important, with decades of strong and steady jet being interspersed with decades of a weak and more variable jet (Woollings et al, 2018; Simpson et al, 2019; Osman et al, 2021). Therefore, identifying the impact of global warming on the jet has remained elusive and controversial (Barnes and Screen, 2015). Even though there is a broad agreement on the poleward shift of the eddy-driven jet with global warming (Pena-Ortiz et al, 2013; Woollings et al, 2014; Lee et al, 2021), the impact of global warming on the other characteristics of the jet are still unclear (Stendel et al, 2021). Indeed, the jet has been caught in the 'tug-of-war' (Held, 1993) between two competing phenomena: the Arctic amplification (AA) and the tropical upper-tropospheric warming.

As the Arctic is warming more rapidly than the rest of the world (Cohen et al, 2018) – reducing the Arctic-to-mid-latitude geopotential gradient – it has been argued that this could lead to changes in the configuration of the jet stream (Francis and Vavrus, 2015). The reduced equator-to-pole temperature

73 gradient could weaken the predominant westerly winds, which, in turn, could
74 cause larger-amplitude waves in the midlatitude circulation. However, global
75 warming also leads to tropical upper-tropospheric warming, which would in
76 contrary act to increase the equator to pole gradient of temperature, rein-
77 forcing the jet (Stendel et al, 2021). Another mechanism could increase the
78 waviness of the jet: the increased land-sea gradients under global warming, as
79 supported by the recent theoretical work of Moon et al (2022).

80 Changes in the latitudinal or longitudinal temperature gradients are how-
81 ever not the only mechanisms through which the dynamics of the jet could have
82 changed during the 20th century. Anthropogenic aerosols emissions and inter-
83 nal variability of the climate system are two other competing factors. Several
84 studies have demonstrated the role of anthropogenic aerosols in changing the
85 dynamics of the North Atlantic atmosphere (e.g. Pausata et al (2015); Diao
86 and Xu (2022); Murakami (2022)) through anomalous heating or cooling in
87 the mid-latitudes. Low frequency variability of the ocean is another confound-
88 ing phenomenon. The Atlantic Multidecadal Oscillation (AMO), a 60–80 year
89 basinwide quasi-oscillation in North Atlantic sea surface temperatures (Kerr,
90 2000), can be invoked to explain the interdecadal changes in the dynamics of
91 the jet. The variations in the coupled El-Nino-Southern Oscillation (ENSO)
92 and Pacific Decadal Oscillation (PDO) could also influence the variability of
93 the jet through the generation of Rossby wave trains (Ding et al, 2017; Mezzina
94 et al, 2020).

95 Studies on reanalysis data have shown conflicting results on the evolution
96 of jets under global warming with some of them concluding to a weakening of
97 the North Atlantic jet (Francis and Vavrus, 2015; Coumou et al, 2015; Harvey
98 et al, 2020), while others concluded to a stronger jet under global warming
99 (Iqbal et al, 2018; Tenenbaum et al, 2022; Hallam et al, 2022). Some studies
100 have also targeted directly the measurement of the "waviness" of the mid-
101 latitude circulation, with various metrics (Cattiaux et al, 2016; Peings et al,
102 2018; Blackport and Screen, 2020). A common theme of those studies is that
103 the natural variability of the jet stream may be a sufficient explanation to
104 the recent observed increases of its waviness (Osman et al, 2021; Blackport
105 and Screen, 2020). Therefore, the recent observed covariability between wavi-
106 ness and temperature gradients on interannual to decadal time scales may not
107 represent a forced response.

108 Here, we address the question of quantifying the changes in the character-
109 istics of the Euro-Atlantic eddy-driven jet stream due solely to global warming
110 over the 20th century.

111 Several approaches have been developed to detect the eddy-driven jet
112 stream position from wind and pressure maps, each with advantages but also
113 limitations. Some algorithms were developed to capture the 3D (Limbach et al,
114 2012) or 2D structure (Molnos et al, 2017; Spensberger et al, 2017) of the jet.
115 A large part of the literature investigating the jet variability however reduces
116 the jet to a single point characterized by a latitude, the so-called Jet Latitude
117 Index (JLI), and a wind speed by finding the point where the zonally averaged

low-level zonal wind is maximum (Woollings et al, 2010). This method provides useful insights and is very handful to make time-series statistics using only two indexes, nonetheless it misses key geometric features of the jet such as the omega-shaped pattern associated with blocking events. Here we adopt a more geometric view by considering the latitudinal position of the jet at each longitude (Faranda et al, 2019b).

We analyze this representation of the jet with recently developed indicators (Lucarini et al, 2016; Faranda et al, 2017; Messori et al, 2021) based on dynamical systems theory. We expand the results of Faranda et al (2019a) and Rodrigues et al (2018) who have shown the interest of using time series of these indicators to detect changes in the large scale circulation. Here we target specifically the eddy-driven jet. We finally employ a causal framework (Kretschmer et al, 2021) based on the existing climate knowledge to control for the influence of confounding factors – internal variability and anthropogenic aerosols emissions – and quantify the sole effect of global warming on various indicators of the jet variability.

This paper is organized as follows: in Section 2, we introduce the data used and the methods developed to detect the jet stream position and quantify its variability. In Section 3, we assess the ability of our indicators to characterize the jet variability by investigating how they are related to other jet characteristics. We also show the relevance of targeting specifically the jet as an atmospheric feature rather than studying sea-level pressure or geopotential maps. In Section 4, we investigate the interdecadal variability of the eddy-driven jet over the 20th century and relate it to classical indices of natural variability. Finally, the discussion of the results and the conclusions drawn from our analysis are presented in section 5.

2 Data and methods

2.1 Data

The analyses proposed here are based on the ERA5 reanalysis data of the European Centre for Medium range Weather Forecasts (Hersbach et al, 2020). We use daily averaged fields with a 0.25° horizontal resolution over the 1950–2021 period for the Euro-Atlantic region from 22.5°N to 70°N in latitude and from 80°W to 50°E in longitude. For disentangling the role of natural and forced response on the low-frequency evolution of the jet variability, we use the ERA20C reanalysis dataset, which is the 20th century reanalysis of the ECMWF (Poli et al, 2016), over the 1900–2010 period with the same spatial extension. This dataset has a resolution of 1.125° . For both data sets, the variables considered are the daily-averaged geopotential height at 500hPa (Z500), sea-level pressure (SLP) and horizontal wind speed between 850 and 700hPa.

For quantifying the link between the variability of the jet position, classical indices of natural variability and global warming, we use monthly indices downloaded from the Climate Explorer web tool. For the AMO, we use the

161 AMO index of the Met Office Hadley Centre/Climatic Research Unit (van
162 Oldenborgh et al, 2009). This index corresponds to the average of monthly Sea
163 Surface Temperature (SST) anomalies with respect to the ensemble mean of
164 the reanalysis over the North Atlantic. For the PDO, we use the PDO index
165 of the Hadley Center based on an EOF decomposition of Pacific SSTs. For the
166 ENSO we take the Nino 3.4 index, which is the area averaged SST from 5S-5N
167 and 170-120W (Van Oldenborgh et al, 2021). For quantifying global warming,
168 we use the monthly global mean Earth surface temperature anomalies (rel-
169 ative to the 1961–1990 period) provided by the Hadley Centre (HadCRUT5
170 data set, Morice et al (2021)). For the AMO, PDO and ENSO indices a linear
171 trend has been removed to account for the global warming signal.

172 We further consider the impact of aerosols forcing. We use the ambient
173 aerosol absorption optical thickness at 550nm provided at a monthly time
174 scale by the IPSL model (Dufresne et al, 2013) under the CMIP5 historical
175 configuration for the 1900-2000 period and under the RCP4.5 scenario for
176 the period 2000-2020. The optical thickness is provided at each grid point
177 and we average the field over the same Euro-Atlantic sector as for ERA5 and
178 ERA20C. The ERA5 and ERA20C reanalyses both use the CMIP5 forcing
179 files for aerosols concentration (Poli et al, 2016; Hersbach et al, 2020), which
180 consists of monthly 10 year-averaged files.

181 2.2 Detecting the jet position

182 For detecting the jet position, we first average over 850–700hPa pressure levels
183 the horizontal wind speed. Contrary to Woollings et al (2010), we investigate
184 the variability of the jet not only over the North Atlantic ocean. In order to
185 avoid boundary layer effects over continental Europe we prefer to begin the
186 averaging process at a higher pressure level: 850hPa rather than 925hPa. We
187 then apply a 10 days low-pass Lanczos filter with a window of 61 days to
188 remove the influence of transient eddies (Duchon, 1979). At this point we do
189 not apply a zonal mean but take a two-step approach close to the procedure
190 used by Faranda et al (2019b). The first step consists in finding, for each
191 longitude, the latitude at which the wind horizontal kinetic energy $E = \frac{1}{2}\vec{u}_H^2$
192 is maximum. The second step is to apply a 25° of longitudes rolling median to
193 the previous positions. This rolling median is applied to avoid a nonphysical
194 detection of breaks in the jet. With a 0.25° horizontal resolution for ERA5
195 and considering the low-level jet, the algorithm sometimes detects high-wind
196 speeds in the lee of mountains. 25° of longitudes approximately corresponds
197 to 2000km at 45°N, which is also the typical size of mid-latitude baroclinic
198 disturbances (Hoskins and James, 2014) so that we consider that this rolling
199 median has a physical basis. An example of the jet position found with this
200 method is given in figure 1.

201 Our approach considers the jet position as a vector of positions indexed
202 by longitudes. However, vectors are not easy to study as time series and we
203 need to reduce the dimension to summarize these objects to single values. The
204 following sections present the indicators we used.

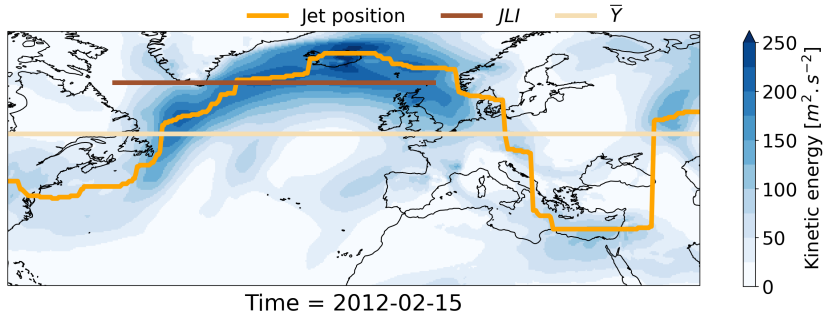


Fig. 1 Snapshot of the horizontal wind kinetic energy and jet position for one example day. Wind horizontal kinetic energy $E = \frac{1}{2}\bar{u}_H^2$ (colors) and jet position found by the algorithm (orange line). The yellow and brown lines represent respectively the jet latitude index JLI and the mean position of the jet \bar{Y} found with our method.

2.3 Dynamical indicators

In physics, dynamical systems can be defined as objects whose states vary with time. In atmospheric physics in particular, fields such as sea-level pressure, temperature or precipitation can be considered as observables of a dynamical system, namely the atmospheric flow (Lucarini et al, 2016; Faranda et al, 2017). In our case, the observable we are studying is the jet position at each longitude, going through different daily states, noted ζ . A state of our system can be described as a vector of dimension lon where lon represents the number of grid points along the longitudinal axis. The y^{th} position in this vector contains the latitudinal value of the jet position for the y^{th} longitude. The ensemble of states of the jet at all time approximate the dynamics of the atmospheric flow and should retain some of the properties of the full, high dimensional, attractor of mid-latitude atmospheric motions.

We define two indicators to characterize our dynamical system: the local dimension d and the local persistence θ^{-1} which both characterise instantaneous state of the system in the phase space (Lucarini et al, 2016; Faranda et al, 2017). Both of these indicators are computed using the fact that the probability for a recurrence of a system configuration (a state) can be linked to the generalized Pareto distribution (Pickands, 1975). To compute this probability from data, we compute the series of distances $dist(x(t), \zeta)$ between a state of the system ζ and all other points $x(t)$ on the trajectory of the system. This time series of distances is then transformed into: $g(t) = -\log(dist(x(t), \zeta))$ so that being close to state ζ is equivalent to exceeding a threshold $s(q)$ where q is a percentile of the series $g(t)$. We use the 98% percentile of all values of $g(t)$, which ensures to have enough data while keeping only the extremes. For the calculation of the distances between states, we use the Euclidian distance. It can be shown that the probability distribution of $g(t)$ when it exceeds $s(q)$ converges to a Pareto distribution (Lucarini et al, 2016) with scale parameter σ , and a shape parameter $\xi = 0$.

234 The local dimension d is practically estimated as the inverse of the scale
 235 parameter of the generalized Pareto distribution fitted on the data which sat-
 236 isfies $g(t) > s(q)$. d is a proxy for the system's active number of degrees of
 237 freedom when reaching a region of phase space. Thus, even when considering
 238 a system with a large number — possibly infinite — of dimensions, d pro-
 239 vides the local number of dimensions that the system can be summarized to.
 240 Therefore a state 1 with a local dimension d_1 greater than the local dimen-
 241 sion d_2 of another state 2 means that the behavior of the system around state
 242 1 has more dimensions on which to evolve and is therefore less predictable
 243 than around state 2 (Messori et al, 2017; Hochman et al, 2019). Additionally,
 244 Pons et al (2020) showed that d can be used as a measure of co-dependance:
 245 a high degree of synchronization between the variables defining the system is
 246 associated with a low value of d .

247 The second dynamical system indicator we use is the persistence θ^{-1} of
 248 a given state ζ , which is equivalent to the mean residence time of the tra-
 249 jectories when they enter the neighborhood of ζ . This metric corresponds to
 250 the inverse of a well defined statistical quantity introduced in extreme value
 251 statistics, namely the extremal index θ . The latter is here estimated using the
 252 Süveges (2007) estimator on the time series $g(t)$. Note that in the framework
 253 of dynamical systems, we find $\theta = 0$ at stable fixed points of the dynamics
 254 (the trajectory resides an infinite amount of time in the neighborhood of this
 255 state), with an infinite number of infinitely time resolved trajectories. Con-
 256 versely, $\theta = 1$ is found at non persistent states of the dynamics (see Moloney
 257 et al (2019) for more details). In general, for time-continuous systems sampled
 258 at a given resolution dt , $\theta^{-1} > 1$. For daily sea-level pressure fields over the
 259 North Atlantic, Faranda et al (2017) found θ^{-1} values varying between 2 and
 260 3 days. One may note that these values depend on the size and the timestep
 261 of the data set used, and on the chosen percentile q . Therefore the local per-
 262 sistence θ^{-1} is to be used to compare different states within the same data
 263 set.

264 2.4 Other variability indicators

265 To the local dimension d and persistence θ^{-1} indicators we add three other
 266 indicators of the jet stream state for analysing its variability. For each day we
 267 compute :

- 268 • the jet mean position \bar{Y} , defined as the zonal average of the jet positions
 269 found with the detection algorithm. As illustrated in Fig. 1 one should note
 270 that this indicator is not equivalent to the JLI for two reasons: (i) our
 271 indicator is computed on the full Euro-Atlantic sector and not only over the
 272 North Atlantic and (ii) the mean position is computed without applying a
 273 zonal average to zonal wind speed;
- 274 • the jet mean speed \bar{U} , defined as the zonal average of the norm of the
 275 horizontal wind vector \vec{u}_J at the jet position: $\bar{U} = \frac{1}{lon} \sum_{lon} \sqrt{u_J^2 + v_J^2}$. For
 276 each longitude, the horizontal wind vector \vec{u}_J is computed as the mean

277 of horizontal wind vectors within a 2.5° latitudinal extent around the jet
 278 position. Again, this indicator is not equivalent to the zonal jet speed as
 279 defined in [Woollings et al \(2010\)](#);

- 280 • the jet waviness W , defined as the longitudinal standard deviation of the
 281 jet position. Before computing this parameter, we remove a linear spatial
 282 trend to the jet position as the jet has a tendency to present a northward
 283 tilt over the North Atlantic. This indicator is always positive and indicates
 284 a jet without (with) meanders when taking low (high) values.

285 In addition to our indicator \bar{Y} and \bar{U} , we also use the more classical jet
 286 latitude index JLI and zonally-averaged zonal wind speed U_{JLI} . There is no
 287 universally accepted metric to measure the "waviness" of mid-latitude circula-
 288 tion and therefore several measures have been used in the literature ([Blackport
 289 and Screen, 2020](#)). Our measure of waviness W is straightforward to compute,
 290 intuitive and gives easily interpretable results. We note that our approach is
 291 close to the sinuosity metric proposed by [Cattiaux et al \(2016\)](#).

292 3 Diagnosing the jet variability

293 [Faranda et al \(2017\)](#) made the case for the use of dynamical indicators to
 294 investigate the weather variability over the Euro-Atlantic sector with the tools
 295 presented in 2.3 using SLP as a state vector. Here we specifically target the
 296 jet position ([Faranda et al, 2019b](#); [Messori et al, 2021](#)). Figure 2 presents
 297 the cross distribution of d and θ^{-1} computed on SLP, Z500 and jet positions
 298 reanalysis data over the Euro-Atlantic sector. The dynamical indicators for
 299 SLP and Z500 are strongly correlated (Pearson correlation coefficient $r = 0.45$
 300 for d and $r = 0.71$ for θ^{-1}), which was expected in so far as those fields carry
 301 similar information about the synoptic meteorological state of the atmosphere.
 302 Conversely, almost no correlation is observed between the dynamical indicators
 303 computed on the jet position and the one computed on the SLP or the Z500.
 304 As previously, this illustrates that the variability of the jet position cannot
 305 be reduced to the variability of the SLP and Z500 fields ([Dorrington and
 306 Strommen, 2020](#)).

307 The absolute values of the indicators can be compared from one data set
 308 to another in so far as they have a similar sampling frequency. The mean
 309 local dimension found for the ERA5 data set is 7.6. With a different spatial
 310 resolution (0.25° vs 1.125°), we find a mean value of 7.5 for the ERA20C data
 311 set. These values must be compared with the values of 11.4 and 13.5 for the
 312 mean local dimension of the Z500 and SLP fields on the ERA5 data set. For the
 313 persistence, we find values evolving in the same range for the three variables
 314 (between 2 and 3 days).

315 Figure 3 panel (c) displays the cross distribution of points for the dynamical
 316 indicators d and θ^{-1} computed on the jet position vectors. The marginal
 317 distributions are shown in Fig. 3 panel (a) and (d). The points are colored
 318 with respect to which tercile of the distribution of the waviness indicator W
 319 they belong to (Fig. 3 panel (b)). The less wavy jets are associated with high

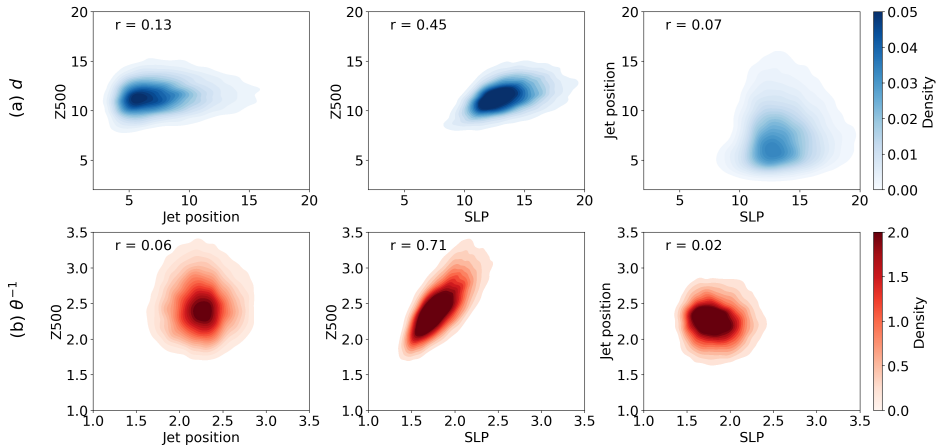


Fig. 2 Cross distributions of dynamical indicators for Z500, SLP and jet positions (ERA5). (a) Cross distributions of the local dimension d between the Z500 field and jet position, the Z500 field and the SLP field, and jet position and the SLP field. (b) Cross distributions of the local persistence θ^{-1} between the Z500 field and jet position, the Z500 field and the SLP field, and jet position and the SLP field. For computational reasons, the dynamical indicators on the Z500 and the SLP fields have been computed with a spatial resolution of 0.5° instead of 0.25° .

320 values of θ^{-1} and low values of d while the most wavy jets are found to have
 321 lower values of θ^{-1} and higher values of d . These results are consistent with
 322 what Messori et al (2021) found using an idealised quasi-geostrophic model
 323 and computing indicators on the wind field. Figure 9 and 10 in annex present
 324 the same analysis for the \bar{U} and \bar{Y} indicators. Contrary to Fig. 3, the d and
 325 θ^{-1} indicator have difficulties discriminating the jet dynamical behavior when
 326 using the mean speed and mean position, which suggests that \bar{U} and \bar{Y} are not
 327 the most relevant indicators to capture the dynamical properties of the jet.

328 As in Faranda et al (2017) and Messori et al (2017), to better under-
 329 stand what kind of dynamical information the indicators reveal, we analyze
 330 the extreme cases of the d and θ^{-1} indicators. We take the composite maps
 331 over the days belonging to the top 2% in term of one of the indicator and for
 332 which the other one is not extreme (in the sense that it does not belong to the
 333 top 2% neither to the bottom 2% quantiles). We define four situations: low
 334 local dimension (N=377 days of observations), high local dimension (N=458
 335 days of observations), low local persistence (N=457 days of observations) and
 336 high local persistence (N=357 days of observations), which are presented in
 337 Figure 4.

338 In the high local dimension case, the synoptic meteorological situation
 339 shows no clear pattern, and the density of the jet position is widespread. This
 340 behavior is consistent with the concept of local dimension: for points with a
 341 very high local dimension, the system has many degrees of freedom and can
 342 correspond to many dynamical situations. In the low local dimension case,
 343 the density of the jet stream position shows a bi-modality over the eastern

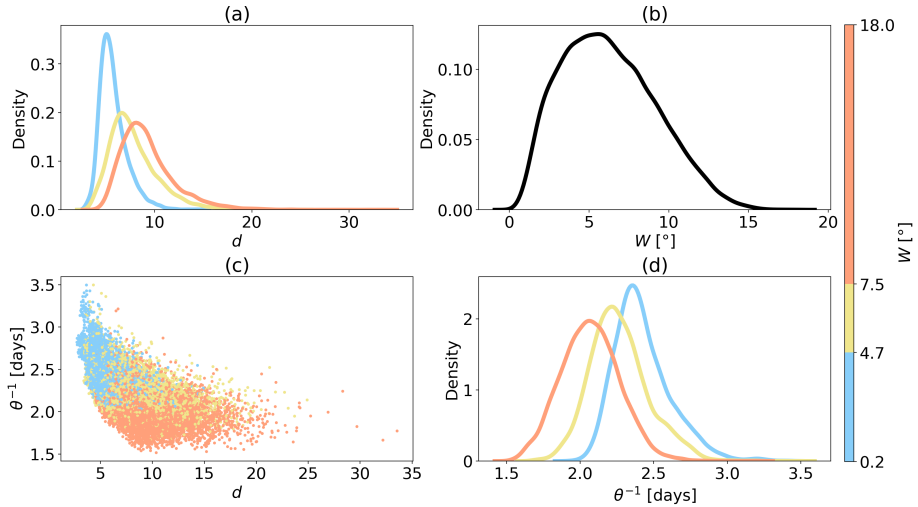


Fig. 3 Link between the dynamical indicators and the jet waviness (ERA5). (a) Distribution of local dimension d for the three terciles of the waviness W . (b) Distribution of W . (c) Cross distribution of d and θ^{-1} colored by the tercile of the W indicator. (d) Distribution of local persistence θ^{-1} for the three terciles of the waviness W .

344 part of the American continent and a tri-modality over the European continent,
 345 leading to five distinct clusters of trajectories. The two main modes
 346 represented by black dashed lines count for approximately 60% of all the trajec-
 347 tories. The synoptic situation displays a large anticyclone over North-Western
 348 Europe reminiscent of the NAO+ weather regime but is associated with several
 349 possible patterns of the jet.

350 In the low local persistence case, the anomalies of SLP show a pattern, close
 351 to the Scandinavian Blocking situation. The averaged jet pattern is peculiar
 352 but nonetheless well defined – in so far as there is a low dispersion of the
 353 jet position density – and has a pronounced dip over the Mediterranean Sea
 354 in its main mode (80% of the trajectories). This very wavy situation of the
 355 jet is reminiscent of recent synoptic situation corresponding to temperature
 356 extremes over Western Europe (e.g. Mitchell et al (2019)). Finally, the high
 357 local persistence case is reminiscent of the NAO- situations with a positive
 358 SLP anomaly over Greenland and a negative slp anomlay over the Azores
 359 (Michelangeli et al, 1995).

360 We now turn to using these indicators to study the recent past evolution
 361 of the Euro-Atlantic eddy-driven jet stream and its relation to usual modes of
 362 variability of the climate. In the following, we mainly display results based on
 363 the ERA20C data set because it spans a longer time period. The corresponding
 364 results for the ERA5 data set are presented in annex.

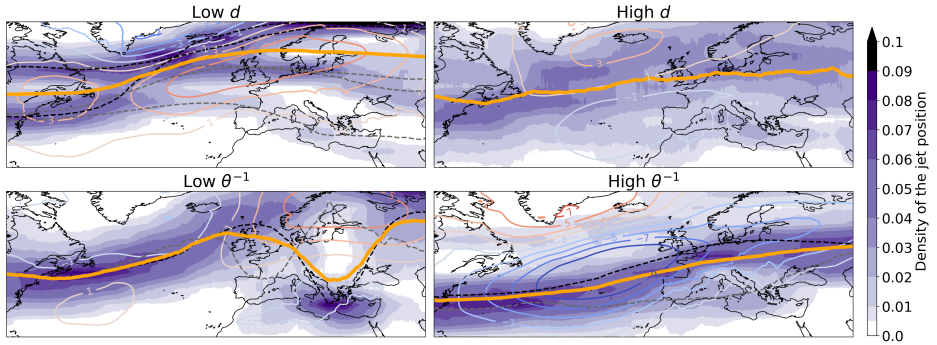


Fig. 4 Extreme d and θ^{-1} situations (ERA5). Composite maps of SLP anomalies in hPa (contours), density of jet positions (colors) and associated mean position (orange lines) for the days with extreme values of the local dimension d and the local persistence θ^{-1} . The black dashed lines are the main modes (more than 30% of the trajectories) and the gray dashed lines are the minor modes (less than 30% of the trajectories).

365 4 Interdecadal variations of the eddy-driven jet 366 stream

367 Figure 6 panels (a) and (b) present the temporal evolution of the one-year
368 rolling mean of the d and θ^{-1} indicators computed on the jet position vectors
369 for the ERA20C reanalysis data set over the 1900-2010 period. A Gaussian
370 filter with a cut-off frequency of 5 years was applied on the raw time series for
371 obtaining the smoothed time series. The 5 years cut-off frequency was chosen to
372 average out most inter-annual variability (e.g. ENSO). Both indicators display
373 substantial inter-annual variability, up to $\sim 30\%$ (6.5 to 8.5) with respect to
374 its mean for local dimension but only $\sim 10\%$ with respect to its mean for local
375 persistence (3.5 to 3.8). When computing the wavelet spectrum on the raw
376 time series of our indicators (panel (c)) one sees a strong peak at the one year
377 period, which corresponds to the annual cycle. For higher periods, the log-
378 log plot shows that the indicators behave as red noises (straight line), except
379 around the 50 years period where a dominant peak emerges. We ran a similar
380 spectrum analysis over the 1950-2020 period for the ERA5 data set and found
381 a similar peak around the 50 years period (Fig. 11). This peak is also seen
382 when using other indicators (Fig. 5). Nonetheless, a 50 year period in a 110
383 (or 70) years data set is near the limit of detectability, therefore we cannot
384 assert that this is a relevant feature of the jet variability.

385 Fig. 6 panel (a) displays a decrease of local dimension from 1970 to 1990
386 and then an increase up to 2000. This interdecadal variation is large even after
387 applying a 5-year low pass filter ($\sim 10\%$ of the mean value). A well documented
388 phenomenon occurred in the North Atlantic ocean during the period 1970-
389 2000 (Sutton and Dong, 2012; Robson et al, 2016; Jackson et al, 2022). The
390 European climate experienced substantial changes, with anomalously mild,
391 wet, summers in Northern Europe, and hot, dry, summers in Southern Europe.
392 This coincided with a major warming of the North Atlantic Ocean due to a

393 strengthening of the Atlantic Meridional Overturning Circulation (AMOC).
 394 On Fig. 11 we also see an increase of inter-decadal variability between the peri-
 395 ods 1950-1980 and 1990-2020. Using a Levene's test (Levene, 1961) to compare
 396 the difference in variance between the two periods, we find significantly differ-
 397 ent ($p < 0.001$) standard deviations between the one-year rolling mean value
 398 of d distributions of the two periods: 0.25 for the 1950-1980 period and 0.33
 399 for the 1990-2020 period.

400 Figure 5 shows the same plot for the \bar{U} , \bar{Y} and W indicators. The mean
 401 speed and position indicators show no peculiar evolution during the 1970-2000
 402 period. The W indicator however seems to display a similar evolution. It should
 403 be noted that these changes in the observed behavior of the North-Atlantic
 404 eddy-driven jet stream between the 1950-1980 and 1990-2010/2020 periods
 405 may be due to different data collection processes. It is indeed well-known that
 406 the so-called satellite era beginning in the 1980s increased by a large factor the
 407 quantity of available data. The large scale structures of the atmosphere are
 408 usually well resolved in reanalysis data (e.g. Slivinski et al (2021)), nonetheless
 409 we cannot completely rule out the possibility that the observed changes are
 410 not physically relevant features of the jet (see (Rodrigues et al, 2018) for a
 411 similar discussion). The purpose of this paper is not to evaluate whether these
 412 changes are artifacts of the data collection process, but one should be cautious
 413 when attributing these results to a real physical behavior of the jet position.

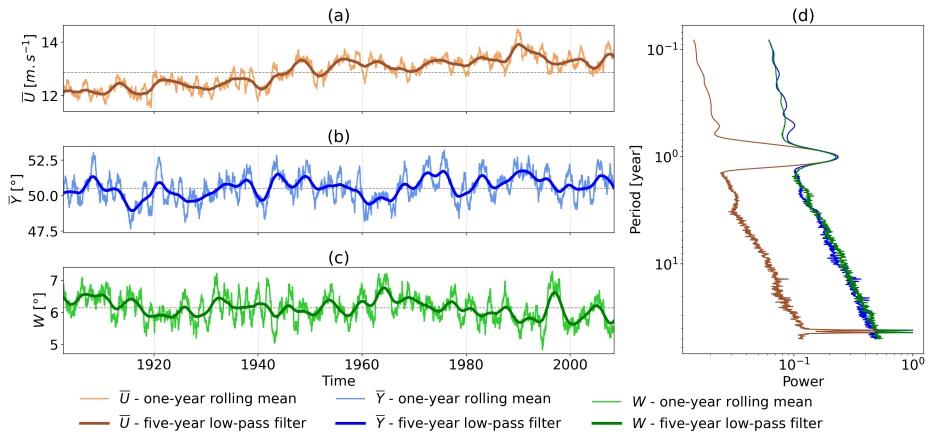


Fig. 5 Time series and power spectrum of \bar{U} , \bar{Y} and W (ERA20C). (a) Time series of \bar{U} with a one-year rolling mean and a five-year low-pass filter. (b) Time series of \bar{Y} with a one-year rolling mean and a five-year low-pass filter. (c) Time series of W with a one-year rolling mean and a five-year low-pass filter. (d) Wavelet spectrum of \bar{U} , \bar{Y} and W .

414 We now wish to estimate the effect of global warming on the variability of
 415 the jet using our dynamical indicators as a relevant measure of "variability".
 416 Isolating the contribution of global warming to the observed changes in the
 417 behavior of the jet is not straightforward in so far as the jet displays a large

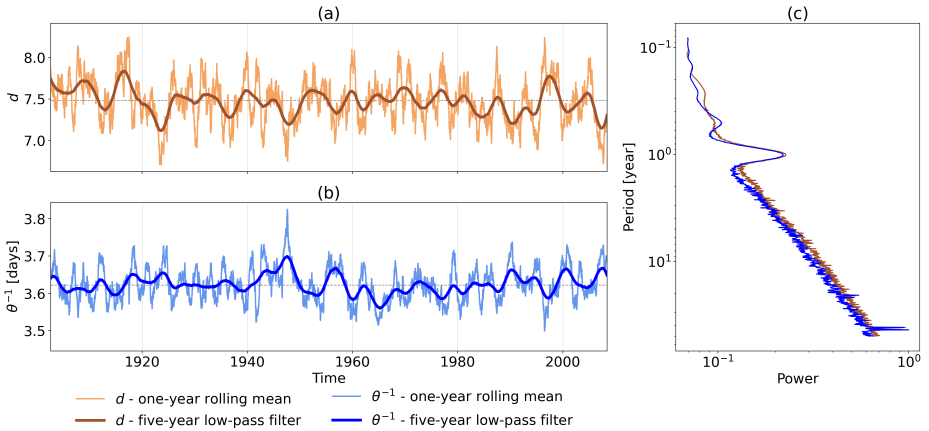


Fig. 6 Time series and power spectrum of d and θ^{-1} (ERA20C). (a) Time series of d with a one-year rolling mean and a five-year low-pass filter. (b) Time series of θ^{-1} with a one-year rolling mean and a five-year low-pass filter. (c) Wavelet spectrum of d and θ^{-1} .

418 variability and any signal of forced change may therefore be obscured by the
 419 influence of other factors. Controlling for these factors would allow to isolate
 420 the global warming signal, but one should take care of controlling only for the
 421 relevant factors. It is necessary to control only for factors that are confounders
 422 of the link between global warming and the variability of the jet (Kretschmer
 423 et al, 2021). Based on existing literature (Newman et al, 2016; Levine et al,
 424 2017; Lin and Qian, 2022), we propose the causal graph depicted in figure 7.
 425 This graph summarizes our hypotheses for quantifying the impact of global
 426 warming on the jet variability on inter-decadal timescales.

427 Potential confounders of the variability of the North-Atlantic eddy-driven
 428 jet stream and global warming are supposed to be the AMO, the ENSO,
 429 the PDO and Aerosols Radiative Forcing (ARF). The variability of the jet is
 430 strongly linked to anomalies of SSTs in the North Atlantic (Simpson et al,
 431 2018), therefore it is natural to posit an impact of the AMO on the jet, even
 432 though here we do not precise what is the exact physical phenomenon by which
 433 the AMO influences the jet. The impact of the ENSO and the PDO on the
 434 Euro-Atlantic climate are also well documented (Ding et al, 2017; Mezzina
 435 et al, 2020), and these two modes influence the inter-decadal variability of the
 436 global temperature of the Earth (Foster and Rahmstorf, 2011). To the natural
 437 variability of the ocean presented by the AMO, the ENSO and the PDO,
 438 we add the ARF over the Euro-Atlantic sector in so far as the changes in the
 439 emissions of aerosols can alter the global circulation (Pausata et al, 2015; Diao
 440 and Xu, 2022; Murakami, 2022). To measure this quantity, we average over the
 441 Euro-Atlantic sector the aerosols optical thickness at 550nm computed using
 442 the IPSL-CM5 model (Dufresne et al, 2013) which uses the same forcing files
 443 as the ERA20C and ERA5 reanalysis. As documented by Qin et al (2020),

444 ARF impacted the AMO over the 20th century, but this mode still has its one
445 variability.

446 One may note that the causal model we are estimating does not show
447 any feedback loop between global warming and the AMO, the PDO and the
448 ENSO. The SSTs of the oceanic regions on which those indicators are com-
449 puted did change during the 20th century in response to the radiative forcing
450 caused by anthropogenic emissions, but here we use the detrended time series
451 of these indicators. We therefore explicitly assume that the global increase
452 of temperature on the Earth had no impacts on the natural evolution of the
453 AMO, PDO and ENSO indicators over the period studied that is not taken
454 into account when removing a linear trend (Trenberth and Shea, 2006). For
455 small increases of the global temperature, this hypothesis is reasonable. How-
456 ever, when extrapolating our results in the future with a much larger warming
457 level, this hypothesis may prove to be wrong.

458 We use monthly-averaged normalized time series and we apply low-pass
459 Gaussian filters with 2, 5 and 10-year cut-off frequencies to ensure robustness
460 with respect to the time-filtering procedure. The rationale for using low-pass
461 filters with cut-off frequencies greater than 2 years is to remove any variations
462 that are irrelevant at the inter-decadal time scale, the main one being the
463 annual cycle. For the filters with 5 and 10-year cut-off frequencies, it may
464 be possible that the ENSO signal is filtered out and therefore we will mainly
465 interpret the results found using the 2-year filter. For simplicity reasons, we
466 choose to estimate a linear model. The model is the following:

$$\text{Jet} = \alpha T + \beta \text{AMO} + \delta \text{PDO} + \gamma \text{ENSO} + \nu \text{ARF} + \epsilon. \quad (1)$$

467 In equation 1, the "Jet" variable represents the different indicators on which
468 we compute the regression. The ϵ term represents a random noise. Even though
469 controlling for the AMO, the PDO, the ENSO and the ARF is essential to
470 estimate the causal effect of T, we stress that their associated coefficients
471 cannot be interpreted as a total causal effect of their respective phenomena
472 on the variability of the jet. We are estimating only a limited part of the
473 causal graph, therefore we only interpret the α coefficient associated with the
474 T parameter.

475 Figure 8 displays the results of the estimation of the α coefficient in
476 equation 1 for the local dimension d , the local persistence θ^{-1} , the mean speed
477 of the jet \bar{U} , the mean position of the jet \bar{Y} , the waviness of the jet W , the jet
478 latitude index JLI and the zonal wind speed at the jet latitude index U_{JLI}
479 using the ERA20C data set over the period 1900-2010. All estimated coeffi-
480 cients are significant at the 5% level when estimating 95% confidence intervals
481 with a maximum likelihood estimator. Results are stable when applying dif-
482 ferent cut-off frequencies for the low-pass filter. We found that global warming
483 significantly decreases the local dimension d and the waviness W of the jet
484 position. We also found that global warming increases the mean speed \bar{U} and
485 the zonal wind speed U_{JLI} at the JLI. Finally, global warming causes a pole-
486 ward shift of the position of the eddy-driven jet, measured using either the

487 mean position \bar{Y} or the *JLI*. When going back to dimensionalized units, we
 488 estimate that a 1K increase of the global temperature of the Earth leads to
 489 a decrease of 2.3% [1.8,2.9] of the local dimension and 7.0% [5.9,8.0] of the
 490 waviness of the jet position with respect to their mean over the 1900-2010
 491 period. It also leads to an increase of the local persistence by 0.4% [0.2,0.5],
 492 of the mean speed by 10.5% [10.1,10.9], of the zonal wind speed at the JLI
 493 by 11.3% [10.5,12.1], of the mean position by 1.5% [1.2,1.8] and of the JLI by
 494 1.8% [1.3,2.3].

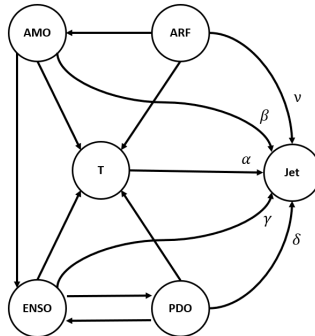


Fig. 7 Estimated causal graph of the influence of global warming on the jet. AMO stands for Atlantic Meridional Oscillation, ENSO for El-Nino Southern Oscillation, PDO for Pacific Decadal Oscillation, ARF for Aerosols Radiative Forcing and T for global mean temperature of the Earth.

495 Figure 12 in annex presents the same analysis using the ERA5 data set over
 496 the 1950-2020 period. Broadly speaking, the estimations of the α coefficient
 497 are much less precise and many coefficients are not statistically different from
 498 zero. The decrease of waviness is still significant when using the 2-year and
 499 5-year filters, but this is not the case for local dimension. The result on local
 500 persistence depends on the filter considered and are overall close to zero. For
 501 jet speed, the mean speed \bar{U} does not seem to be affected by global warming
 502 and the results point towards different directions for U_{JLI} . The northward
 503 shift of the mean position of the jet is better estimated, using either \bar{Y} or *JLI*,
 504 but the significance of the evolution depends on the filter cut-off frequency.

505 5 Discussion and conclusions

506 We studied the variability of the North Atlantic eddy-driven jet stream
 507 described by its instantaneous latitudinal position at each longitude. We used
 508 indicators from dynamical system theory to characterize the underlying attrac-
 509 tor on which the jet is evolving. We showed using that this representation is
 510 more relevant to characterize the jet variability than using the more classi-
 511 cal Z500 and SLP fields and associated weather regimes. Z500 and SLP fields

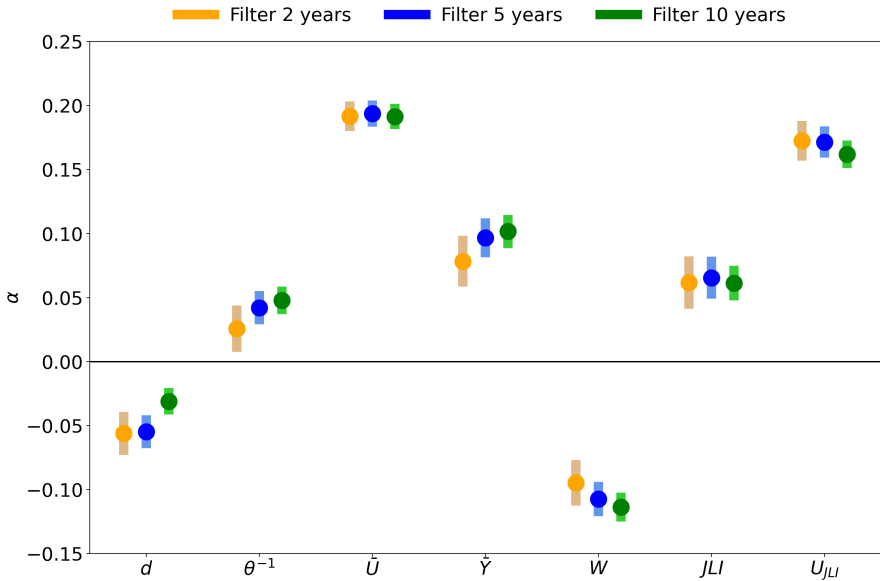


Fig. 8 Estimation of the impact of global warming on indicators of the jet variability (ERA20C). The plot represents the estimated α coefficient for the local dimension d , the local persistence θ^{-1} , the mean speed of the jet \bar{U} , the mean position of the jet \bar{Y} , the waviness of the jet W , the jet latitude index JLI and the zonal wind speed at the jet latitude index U_{JLI} . The dots represent the estimated coefficient and the shaded vertical bars the associated 95% confidence interval. The orange (resp. blue and green) estimation is found using the time series after applying a 2-year (resp. 5-year and 10-year) low-pass Gaussian filter. All time series are monthly averages.

512 carry more information than needed and targeting the jet position per se as
 513 we did allows to focus on the sole dynamics of the jet.

514 We then studied the inter-decadal variability of the jet using the dynamical
 515 indicators. After controlling for potential confounders between the global
 516 temperature of the Earth and the jet, we are able to quantify the impact of
 517 global warming on key indicators of the jet behavior. We showed that, over
 518 the 1900-2010 period, global warming decreased the local dimension and wavi-
 519 ness of the jet position and increased its local persistence. Global warming also
 520 increased the wind speed of the jet and shifted its mean position to the north.
 521 The decrease of waviness and poleward shift results hold using the ERA5 data
 522 set over the period 1950-2020, but this is not the case for the other indicators.

523 [Faranda et al \(2019a\)](#) and [Rodrigues et al \(2018\)](#) also showed a decrease in
 524 local dimension over the North-Atlantic for the SLP field in future warming
 525 scenarios. [Faranda et al \(2019a\)](#) attribute this decrease to the warming of the
 526 ocean. Our results suggest a similar mechanism may apply to the eddy-driven
 527 jet. The poleward shift, strengthening and zonalisation of the Euro-Atlantic
 528 eddy-driven jet stream scenario that we found here is coherent with the recent
 529 work of [Blackport and Screen \(2020\)](#) who found similar results using different
 530 metrics on the mid- and upper-troposphere mid-latitudes circulation. We do

531 find an increase in the variability of the jet over the 1990-2020 period with
532 respect to the 1950-1980 period. However, our regression analysis suggests the
533 recent positive phase of the AMO partially offset the decrease in variability
534 of the eddy-driven jet, leading to this paradoxical observation. This would
535 explain the contradicting results found in the literature on the recent changes
536 of the variability of the jet stream (Francis and Vavrus, 2015; Coumou et al,
537 2015; Harvey et al, 2020).

538 The validity of the results we showed depends crucially on the capacity
539 of the reanalysis data sets to reproduce correctly the behavior of the North-
540 Atlantic eddy-driven jet stream in the past. Even though the large structures of
541 the atmosphere are probably the features best resolved by reanalysis (Slivinski
542 et al, 2021), there is no doubt that the reanalysis over the period 1980-2020,
543 the so-called satellite era, provide much better results than in the previous
544 periods. It is not clear whether we should have more confidence on the results
545 found on the ERA5 data set over the period 1950-2020 or on the ERA20C
546 data set over the period 1900-2010. The properties of the jet are probably
547 closer to reality in the first data set but the natural variability of the climate
548 system is better sampled in the second. Therefore, even though we used a
549 causal inference framework to disentangle the influence of confounders from
550 the influence of global warming of the Earth on the jet, we cannot assert that
551 our results give the causal impact of global warming on the variability of the
552 jet.

553 Finally, our results demonstrate the interest of using tools from dynamical
554 system theory to target specific patterns of the large scale atmospheric cir-
555 culation and quantify their natural and forced variability. We also think that
556 these tools could be used to evaluate whether climate models are able to rep-
557 resent correctly the natural variability of the jet position and we are currently
558 investigating this question.

559 **Acknowledgments.** The authors wish to thank S Charbit, P Yiou, G
560 Messori, T Caby, A Hisi and B Colnet for their fruitful inputs.

561 **Declarations**

- 562 • **Funding:** This work has received support from the European Union's Hori-
563 zon 2020 research and innovation programme under grant agreement No.
564 101003469 (XAIDA), by the European Research Council (ERC) under by
565 the Marie Skłodowska-Curie grant agreement No. 956396 (EDIPI).
- 566 • **Conflict of interest:** The authors declare no conflict of interest.
- 567 • **Ethics approval:** Not applicable.
- 568 • **Consent to participate:** Not applicable.
- 569 • **Consent for publication:** Not applicable.
- 570 • **Availability of data and materials:** The ERA5 and ERA20C are available on
571 the Copernicus web site (<https://cds.climate.copernicus.eu/>). The results of
572 the detection procedure and the time series of indicators are available on
573 demand.

- 574 • Code availability: The main results of this work were obtained using Python.
575 The scripts are available upon request.
- 576 • Authors' contributions: RN designed the analysis. Material preparation,
577 data collection and analysis were performed by VG, AV and RN. All authors
578 contributed to the writing of the paper.

579 Appendix

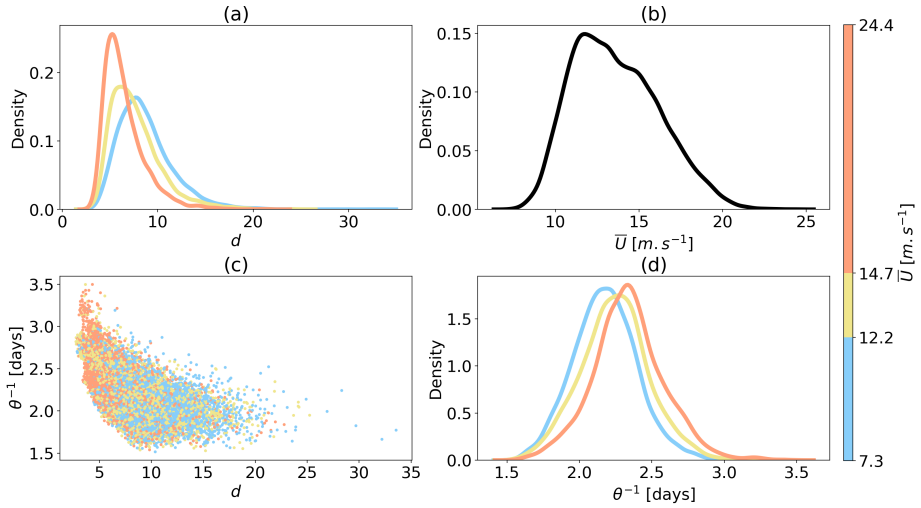


Fig. 9 Link between the dynamical indicators and the jet mean speed. (a) Distribution of local dimension d for the three terciles of the mean speed \bar{U} . (b) Distribution of \bar{U} . (c) Cross distribution of d and θ^{-1} colored by the tercile of the \bar{U} indicator. (d) Distribution of local persistence θ^{-1} for the three terciles of the mean speed \bar{U} .

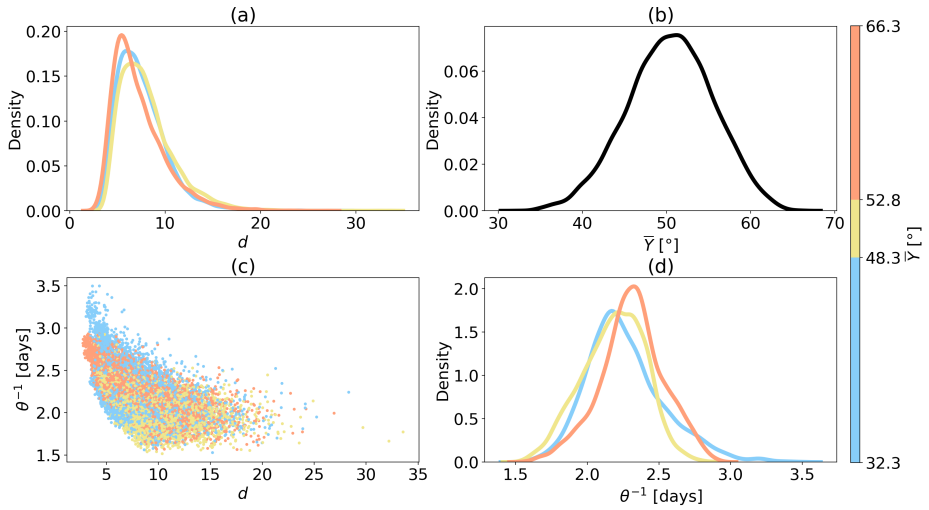


Fig. 10 Link between the dynamical indicators and the jet mean position. (a) Distribution of local dimension d for the three terciles of the mean position \bar{Y} . (b) Distribution of \bar{Y} . (c) Cross distribution of d and θ^{-1} colored by the tercile of the \bar{Y} indicator. (d) Distribution of local persistence θ^{-1} for the three terciles of the mean position \bar{Y} .

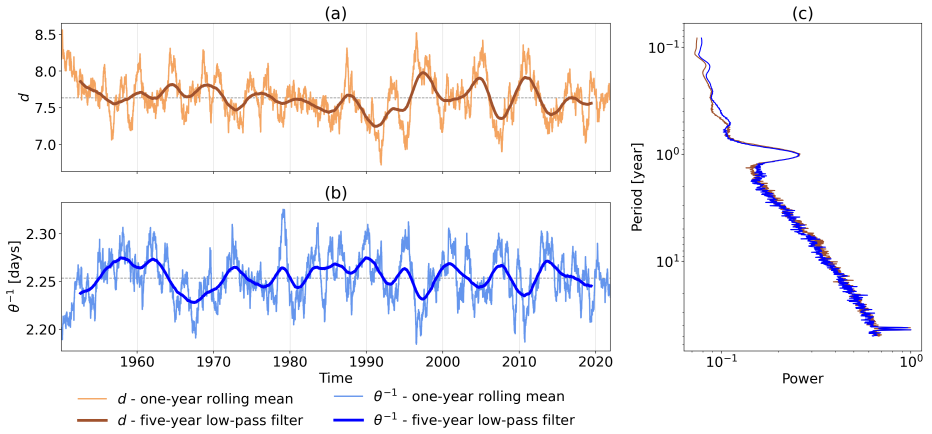


Fig. 11 Time series and power spectrum of d and θ^{-1} (ERA5). (a) Time series of d with a one-year rolling mean and a five-year low-pass filter. (b) Time series of θ^{-1} with a one-year rolling mean and a five-year low-pass filter. (c) Wavelet spectrum of d and θ^{-1} .

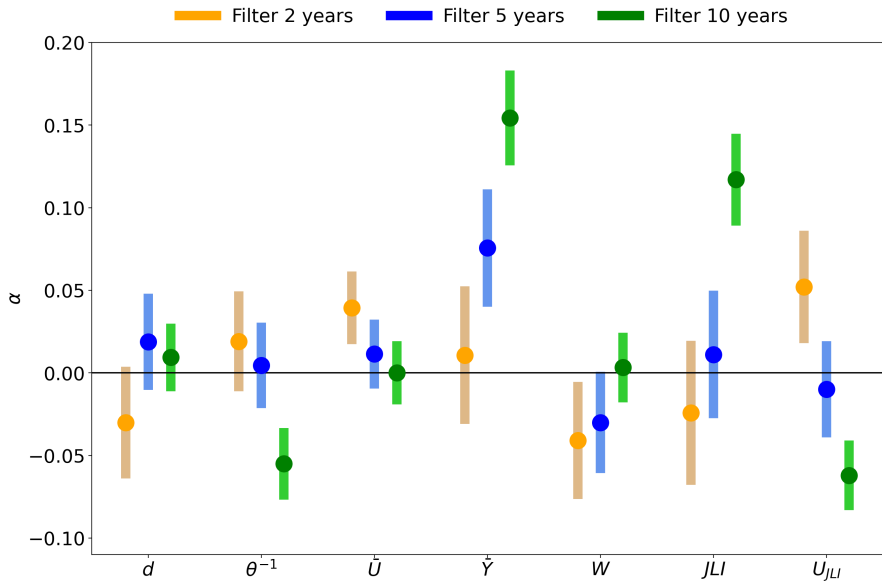


Fig. 12 Estimation of the impact of global warming on indicators of the jet variability (ERA5). The plot represents the estimated α coefficient for the local dimension d , the local persistence θ^{-1} , the mean speed of the jet \bar{U} , the mean position of the jet \bar{Y} , the waviness of the jet W , the jet latitude index JLI and the zonal wind speed at the jet latitude index U_{JLI} . The dots represent the estimated coefficient and the shaded vertical bars the associated 95% confidence interval. The orange (resp. blue and green) estimation is found using the time series after applying a 2-year (resp. 5-year and 10-year) low-pass Gaussian filter. All time series are monthly averages.

References

- 580
- 581 Barnes EA, Screen JA (2015) The impact of arctic warming on the midlatitude
582 jet-stream: Can it? has it? will it? *Wiley Interdisciplinary Reviews: Climate*
583 *Change* 6(3):277–286
- 584 Blackport R, Screen JA (2020) Insignificant effect of arctic amplification
585 on the amplitude of midlatitude atmospheric waves. *Science advances*
586 6(8):eaay2880
- 587 Cattiaux J, Peings Y, Saint-Martin D, et al (2016) Sinuosity of midlati-
588 tude atmospheric flow in a warming world. *Geophysical Research Letters*
589 43(15):8259–8268
- 590 Charney J (1947) The dynamics of long waves in a baroclinic. *Westerly*
591 *Current, J Meteorol* 4
- 592 Cohen J, Zhang X, Francis J, et al (2018) Arctic change and possible influence
593 on mid-latitude climate and weather: a us clivar white paper. *US CLIVAR*
594 *reports*
- 595 Coumou D, Lehmann J, Beckmann J (2015) The weakening summer circula-
596 tion in the northern hemisphere mid-latitudes. *Science* 348(6232):324–327
- 597 Diao C, Xu Y (2022) Reassessing the relative role of anthropogenic aerosols
598 and natural decadal variability in driving the mid-twentieth century global
599 “cooling”: a focus on the latitudinal gradient of tropospheric temperature.
600 *Climate Dynamics* pp 1–27
- 601 Ding S, Chen W, Feng J, et al (2017) Combined impacts of pdo and two types
602 of la niña on climate anomalies in europe. *Journal of climate* 30(9):3253–3278
- 603 Dorrington J, Strommen K (2020) Jet speed variability obscures euro-atlantic
604 regime structure. *Geophysical Research Letters* 47(15):e2020GL087,907
- 605 Duchon CE (1979) Lanczos filtering in one and two dimensions. *Journal of*
606 *Applied Meteorology and Climatology* 18(8):1016–1022
- 607 Dufresne JL, Foujols MA, Denvil S, et al (2013) Climate change projec-
608 tions using the ipsl-cm5 earth system model: from cmip3 to cmip5. *Climate*
609 *dynamics* 40(9):2123–2165
- 610 Faranda D, Messori G, Yiou P (2017) Dynamical proxies of north atlantic
611 predictability and extremes. *Scientific reports* 7(1):1–10
- 612 Faranda D, Alvarez-Castro MC, Messori G, et al (2019a) The hammam effect
613 or how a warm ocean enhances large scale atmospheric predictability. *Nature*
614 *Communications* 10:1316

- 615 Faranda D, Sato Y, Messori G, et al (2019b) Minimal dynamical systems model
616 of the northern hemisphere jet stream via embedding of climate data. *Earth*
617 *System Dynamics* 10(3):555–567
- 618 Foster G, Rahmstorf S (2011) Global temperature evolution 1979–2010.
619 *Environmental research letters* 6(4):044,022
- 620 Francis JA, Vavrus SJ (2015) Evidence for a wavier jet stream in response to
621 rapid arctic warming. *Environmental Research Letters* 10(1):014,005
- 622 Hallam S, Josey SA, McCarthy GD, et al (2022) A regional (land–ocean)
623 comparison of the seasonal to decadal variability of the northern hemisphere
624 jet stream 1871–2011. *Climate Dynamics* pp 1–22
- 625 Harvey B, Cook P, Shaffrey L, et al (2020) The response of the northern hemi-
626 sphere storm tracks and jet streams to climate change in the cmip3, cmip5,
627 and cmip6 climate models. *Journal of Geophysical Research: Atmospheres*
628 125(23):e2020JD032,701
- 629 Held IM (1975) Momentum transport by quasi-geostrophic eddies. *J Atmos*
630 *Sci* 32(7):1494–1497
- 631 Held IM (1993) Large-scale dynamics and global warming. *Bulletin of the*
632 *American Meteorological Society* 74(2):228–242
- 633 Held IM, Hou AY (1980) Nonlinear axially symmetric circulations in a nearly
634 inviscid atmosphere. *Journal of the Atmospheric Sciences* 37(3):515–533
- 635 Hersbach H, Bell B, Berrisford P, et al (2020) The era5 global reanalysis.
636 *Quarterly Journal of the Royal Meteorological Society* 146(730):1999–2049
- 637 Hochman A, Alpert P, Harpaz T, et al (2019) A new dynamical systems
638 perspective on atmospheric predictability: Eastern mediterranean weather
639 regimes as a case study. *Science advances* 5(6):eaau0936
- 640 Holton JR (1973) An introduction to dynamic meteorology. *American Journal*
641 *of Physics* 41(5):752–754
- 642 Hoskins BJ, James IN (2014) *Fluid dynamics of the mid-latitude atmosphere.*
643 *John Wiley & Sons*
- 644 Hurrell JW, Deser C (2010) North atlantic climate variability: the role of the
645 north atlantic oscillation. *Journal of marine systems* 79(3-4):231–244
- 646 Iqbal W, Leung WN, Hannachi A (2018) Analysis of the variability of the north
647 atlantic eddy-driven jet stream in cmip5. *Climate Dynamics* 51(1):235–247

- 648 Jackson LC, Biastoch A, Buckley MW, et al (2022) The evolution of the North
649 Atlantic Meridional Overturning Circulation since 1980. *Nature Reviews*
650 *Earth & Environment* 3:241–254
- 651 Kautz LA, Martius O, Pfahl S, et al (2022) Atmospheric blocking and weather
652 extremes over the euro-atlantic sector—a review. *Weather and Climate*
653 *Dynamics* 3(1):305–336
- 654 Kerr RA (2000) A north atlantic climate pacemaker for the centuries. *Science*
655 288(5473):1984–1985
- 656 Kretschmer M, Adams SV, Arribas A, et al (2021) Quantifying causal path-
657 ways of teleconnections. *Bulletin of the American Meteorological Society*
658 102(12):E2247–E2263
- 659 Lee JY, Marotzke J, Bala G, et al (2021) Future Global Climate: Scenario-
660 Based Projections and Near-Term Information. In *Climate Change 2021:*
661 *The Physical Science Basis. Contribution of Working Group I to the Sixth*
662 *Assessment Report of the Intergovernmental Panel on Climate Change.*
663 Cambridge University Press
- 664 Lee S, Kim Hk (2003) The dynamical relationship between subtropical and
665 eddy-driven jets. *Journal of the atmospheric sciences* 60(12):1490–1503
- 666 Levene H (1961) Robust tests for equality of variances. *Contributions to*
667 *probability and statistics Essays in honor of Harold Hotelling* pp 279–292
- 668 Levine AF, McPhaden MJ, Frierson DM (2017) The impact of the amo on
669 multidecadal enso variability. *Geophysical Research Letters* 44(8):3877–3886
- 670 Limbach S, Schömer E, Wernli H (2012) Detection, tracking and event local-
671 ization of jet stream features in 4-d atmospheric data. *Geoscientific Model*
672 *Development* 5(2):457–470
- 673 Lin J, Qian T (2022) The atlantic multi-decadal oscillation. *Atmosphere-Ocean*
674 60(3-4):307–337
- 675 Lucarini V, Faranda D, de Freitas JMM, et al (2016) Extremes and recurrence
676 in dynamical systems. John Wiley & Sons
- 677 Messori G, Caballero R, Faranda D (2017) A dynamical systems approach
678 to studying midlatitude weather extremes. *Geophysical Research Letters*
679 44(7):3346–3354
- 680 Messori G, Harnik N, Madonna E, et al (2021) A dynamical systems character-
681 ization of atmospheric jet regimes. *Earth System Dynamics* 12(1):233–251

- 682 Mezzina B, García-Serrano J, Bladé I, et al (2020) Dynamics of the enso tele-
683 connection and nao variability in the north atlantic–european late winter.
684 *Journal of Climate* 33(3):907–923
- 685 Michelangeli PA, Vautard R, Legras B (1995) Weather regimes: Recurrence
686 and quasi stationarity. *Journal of the atmospheric sciences* 52(8):1237–1256
- 687 Mitchell D, Kornhuber K, Huntingford C, et al (2019) The day the 2003
688 european heatwave record was broken. *The Lancet Planetary Health*
689 3(7):e290–e292
- 690 Molnos S, Mamdouh T, Petri S, et al (2017) A network-based detection scheme
691 for the jet stream core. *Earth System Dynamics* 8(1):75–89
- 692 Moloney NR, Faranda D, Sato Y (2019) An overview of the extremal index.
693 *Chaos: An Interdisciplinary Journal of Nonlinear Science* 29(2):022,101
- 694 Moon W, Kim BM, Yang GH, et al (2022) Wavier jet streams driven by zonally
695 asymmetric surface thermal forcing. *Proceedings of the National Academy*
696 *of Sciences* 119(38):e2200890,119
- 697 Morice CP, Kennedy JJ, Rayner NA, et al (2021) An updated assessment of
698 near-surface temperature change from 1850: the hadcrut5 data set. *Journal*
699 *of Geophysical Research: Atmospheres* 126(3):e2019JD032,361
- 700 Murakami H (2022) Substantial global influence of anthropogenic aerosols on
701 tropical cyclones over the past 40 years. *Science advances* 8(19):eabn9493
- 702 Newman M, Alexander MA, Ault TR, et al (2016) The pacific decadal
703 oscillation, revisited. *Journal of Climate* 29(12):4399–4427
- 704 van Oldenborgh GJ, te Raa LA, Dijkstra HA, et al (2009) Frequency-or
705 amplitude-dependent effects of the atlantic meridional overturning on the
706 tropical pacific ocean. *Ocean science* 5(3):293–301
- 707 Osman MB, Coats S, Das SB, et al (2021) North atlantic jet stream projections
708 in the context of the past 1,250 years. *Proceedings of the National Academy*
709 *of Sciences* 118(38)
- 710 Pausata FSR, Gaetani M, Messori G, et al (2015) The role of aerosol in altering
711 north atlantic atmospheric circulation in winter and its impact on air quality.
712 *Atmospheric Chemistry and Physics* 15(4):1725–1743
- 713 Peings Y, Cattiaux J, Vavrus SJ, et al (2018) Projected squeezing of the
714 wintertime north-atlantic jet. *Environmental Research Letters* 13(7):074,016
- 715 Pena-Ortiz C, Gallego D, Ribera P, et al (2013) Observed trends in the global
716 jet stream characteristics during the second half of the 20th century. *Journal*

- 717 of Geophysical Research: Atmospheres 118(7):2702–2713
- 718 Pickands J (1975) Statistical inference using extreme order statistics.
719 The Annals of Statistics 3(1):119–131. URL [http://www.jstor.org/stable/](http://www.jstor.org/stable/2958083)
720 [2958083](http://www.jstor.org/stable/2958083)
- 721 Poli P, Hersbach H, Dee DP, et al (2016) Era-20c: An atmospheric reanalysis
722 of the twentieth century. Journal of Climate 29(11):4083–4097
- 723 Pons FME, Messori G, Alvarez-Castro MC, et al (2020) Sampling hyperspheres
724 via extreme value theory: implications for measuring attractor dimensions.
725 Journal of statistical physics 179(5):1698–1717
- 726 Qin M, Dai A, Hua W (2020) Quantifying contributions of internal vari-
727 ability and external forcing to atlantic multidecadal variability since 1870.
728 Geophysical Research Letters 47(22):e2020GL089,504
- 729 Rhines PB (1975) Waves and turbulence on a beta-plane. Journal of Fluid
730 Mechanics 69(3):417–443
- 731 Robson J, Ortega P, Sutton R (2016) A reversal of climatic trends in the north
732 atlantic since 2005. Nature Geoscience 9
- 733 Rodrigues D, Alvarez-Castro MC, Messori G, et al (2018) Dynamical proper-
734 ties of the north atlantic atmospheric circulation in the past 150 years in
735 cmip5 models and the 20crv2c reanalysis. Journal of Climate 31(15):6097–
736 6111
- 737 Röthlisberger M, Pfahl S, Martius O (2016) Regional-scale jet waviness modu-
738 lates the occurrence of midlatitude weather extremes. Geophysical Research
739 Letters 43(20):10–989
- 740 Simpson IR, Deser C, McKinnon KA, et al (2018) Modeled and observed
741 multidecadal variability in the north atlantic jet stream and its connection
742 to sea surface temperatures. Journal of Climate 31(20):8313–8338
- 743 Simpson IR, Yeager SG, McKinnon KA, et al (2019) Decadal predictability
744 of late winter precipitation in western Europe through an ocean-jet stream
745 connection. Nature Geoscience 12(8):613–619
- 746 Slivinski L, Compo G, Sardeshmukh P, et al (2021) An evaluation of the
747 performance of the twentieth century reanalysis version 3. Journal of Climate
748 34(4):1417–1438
- 749 Spensberger C, Spengler T (2020) Feature-based jet variability in the upper
750 troposphere. Journal of Climate 33(16):6849–6871

- 751 Spensberger C, Spengler T, Li C (2017) Upper-tropospheric jet axis detection
752 and application to the boreal winter 2013/14. *Monthly Weather Review*
753 145(6):2363–2374
- 754 Stendel M, Francis J, White R, et al (2021) The jet stream and climate change.
755 In: *Climate Change*. Elsevier, p 327–357
- 756 Sutton R, Dong B (2012) Atlantic ocean influence on a shift in european
757 climate in the 1990s. *Nature Geoscience* 5:788–792
- 758 Süveges M (2007) Likelihood estimation of the extremal index. *Extremes*
759 10(1):41–55
- 760 Tenenbaum J, Williams PD, Turp D, et al (2022) Aircraft observations and
761 reanalysis depictions of trends in the north atlantic winter jet stream
762 wind speeds and turbulence. *Quarterly Journal of the Royal Meteorological*
763 *Society*
- 764 Trenberth KE, Shea DJ (2006) Atlantic hurricanes and natural variability in
765 2005. *Geophysical research letters* 33(12)
- 766 Van Oldenborgh GJ, Hendon H, Stockdale T, et al (2021) Defining el niño
767 indices in a warming climate. *Environmental research letters* 16(4):044,003
- 768 Woollings T, Hannachi A, Hoskins B (2010) Variability of the north atlantic
769 eddy-driven jet stream. *Quarterly Journal of the Royal Meteorological*
770 *Society* 136(649):856–868
- 771 Woollings T, Czuchnicki C, Franzke C (2014) Twentieth century north
772 atlantic jet variability. *Quarterly Journal of the Royal Meteorological Society*
773 140(680):783–791
- 774 Woollings T, Barnes E, Hoskins B, et al (2018) Daily to decadal modulation
775 of jet variability. *Journal of Climate* 31(4):1297–1314